

SCIENTIFIC REPORTS



OPEN

High-performance inertial impaction filters for particulate matter removal

Xiaowei Zhang^{1,2}, Wei Zhang³, Mingqiang Yi⁴, Yingjie Wang¹, Pengjun Wang¹, Jun Xu², Fenglei Niu³ & Feng Lin⁵

Airborne particulate matter (PM) is causing more and more serious air pollution and threatening the public health. However, existing air filter technologies with the easy-to-block manner can rarely meet the requirements of high-performance PM filters. Here we propose a conceptually new type of inertial impaction filters for rapidly high-efficiency PM removal. Under the airflow velocity of 8.0 m/s, the real inertial impaction filters show high PM removal efficiencies of up to $97.77 \pm 1.53\%$ and $99.47 \pm 0.45\%$ for $PM_{2.5}$ and PM_{10} , respectively. Compared with the traditional air filters reported previously, the inertia impaction filters exhibit extremely low pressure drop of 5–10 Pa and high quality factor (*QF*) values of 0.380 Pa^{-1} and 0.524 Pa^{-1} for $PM_{2.5}$ and PM_{10} , respectively. These greatly improved *QF* values are achieved through a series of inertial separation processes. The feature dimension of filtration channel is dozens of times larger than PM average size, which greatly decreases airflow resistance. Particularly, this inertial structure can be made of various types of materials, which shows great potential for low-cost fabrication of large-area devices. As a stand-alone device or incorporated with the existing PM air filter, this inertial impaction filter will bring great benefits to the public health.

Air pollutions have raised serious concerns for the public health¹. Among all the noxious pollutants suspended in air, airborne particulate matter (PM), especially particle with an aerodynamic diameter of less than or equal to $2.5 \mu\text{m}$ (referred as $PM_{2.5}$), is the most hazardous air pollution since it can directly be inhaled into the parts of the lung through human nose and bronchi^{2–4}. In particular, long-term exposure to PM air pollutions may result in various respiratory and cardiovascular diseases⁵. Over the past decade, PM air pollution problems become progressively worse, especially in major developing countries, such as China and India. These tiny particles primarily come from vehicle exhausts, coal combustion, biomass burning, and certain industrial processes, which are ever more abundant in most developing countries recently⁵. Until now, the control and removal of PM still remains a great challenge due to its small size and complex variation processes. Figure 1(a) shows two sharp contrast photographs of a location in China during a moderate day (I) and an extremely $PM_{2.5}$ -related hazardous day (II), respectively. During the hazardous air-quality days, the visibility is decreased dramatically and everyone will experience much more serious health effects. A recent report from the Global Burden of Disease (GBD) project of Institute for Health Metrics and Evaluation (IHME) and Health Effects Institute (HEI), indicates that ambient $PM_{2.5}$ contributed to 4.2 million deaths globally and China (1.11 million) and India (1.1 million) each have the highest absolute numbers of deaths in 2015 due to extremely high levels of $PM_{2.5}$ air pollution⁶.

So far, two main types of air filters have been in common use for removing PM particles in air⁷. One is a fibrous air filter, which captures PM particles by the combination of thick physical barriers and adhesion, as shown in Fig. 1(b) (I). In order to maximize filter efficiency, this type of air filter is usually very thick, which inevitably lead to the extremely low air flux with very high pressure drop. Besides, the rapidly weakening and disappearing of static electricity still severely hinders the advancement of this type of air filters with longer working

¹Department of Electrical Engineering and Computer Science, Ningbo University, Ningbo, 315211, China. ²National Laboratory of Solid State Microstructures, Collaborative Innovation Centre of Advanced Microstructures, and Department of Electronic Science and Engineering, Nanjing University, Nanjing, 210093, China. ³Beijing Key Laboratory of Passive Nuclear Power Safety and Technology, North China Electric Power University, Beijing, 102206, China. ⁴Microfluidic Foundry LLC, San Pablo, CA, 94806, United States. ⁵Department of Chemistry, Virginia Tech, VA, 24061, United States. Xiaowei Zhang and Wei Zhang contributed equally to this work. Correspondence and requests for materials should be addressed to P.W. (email: wangpengjun@nbu.edu.cn) or J.X. (email: junxu@nju.edu.cn) or F.N. (email: niufenglei@ncepu.edu.cn)

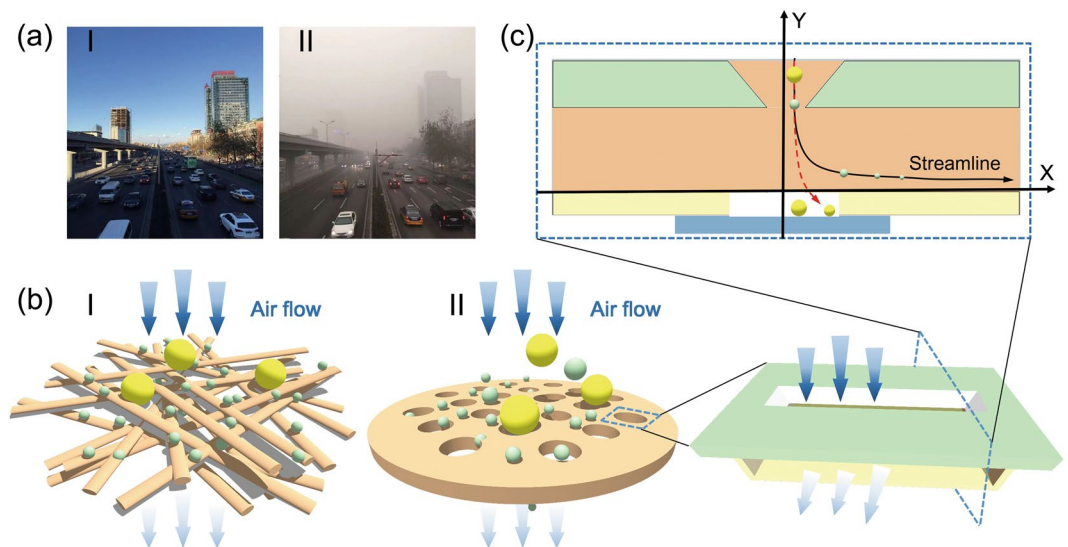


Figure 1. (a) Photographs of a random location in China during (I) a moderate day and (II) an extremely $PM_{2.5}$ -related hazardous day, respectively. (b) Conceptual sketches of two types of existing commercial air filters in common use: (I) a fibrous air filter with static electricity and (II) a membrane air filter with tiny pores. (c) Conceptual illustrations of the basic building block of an inertial impaction filter. Inset is the cross-sectional structure of an inertial impaction filter unit.

life. Another type of air filter is a porous membrane filter based on size exclusion filtration, which is similar to a water filter, as shown in Fig. 1(b) (II). Generally, it can be fabricated by creating tiny pores on a solid substrate or thin film for filtering out PM particles with larger size. To obtain a high filter efficiency, the size of pores should be much smaller, which gives rise to high manufacturing costs and large airflow resistance. Nevertheless, for above two main types of existing commercial air filters, extraordinarily thick filtration channels or extremely tiny filtration pores can inevitably lead to the easy-to-block manners and extremely low air flux. Even worse, some hard PM particles containing a lot of carbon compounds or water molecules, will frequently impact and deform on filter surfaces during the filter process, seriously shortening the service life. Hence, the overall performance of existing air filter technologies, including PM removal efficiency, pressure drop, thermal stability, and service life, can rarely meet the requirements of high-performance air filters.

In order to improve the performance of current air filters, great efforts have been made recently. A series of nanofiber membranes, such as polyvinyl alcohol (PVA)⁸, polyacrylonitrile (PAN)^{9–12}, polyethylene terephthalate (PET)¹³, polyurethane (PU)¹⁴, polylactic acid (PLA)¹⁵, polyamide-66¹⁶, and polyimide (PI)¹⁷, are fabricated and developed to enable strong PM adhesion by effectively controlling the surface chemistry and microstructure of the air filters. Besides, various types of hybrid nanofibers, including PAN/silica¹⁸, polysulfide/titania¹⁹, and PLA/titania²⁰, are constructed to achieve better performance via enhancing electrets effect or roughing surface of nanofibers. Despite recent progresses, these existing nanofiber filters still face the challenge of easy-to-block manner, poor thermal stability and high airflow resistance. Most recently reported low-cost air filters based on electro-spun nanofibers are still easily disabled or destroyed in the hot exhausts from automobile or factory¹⁷. For the existing filtration technologies, the forcing compromise between low airflow resistance and high filter efficiency still inevitably exists. To obtain a higher filter efficiency, the filtration pore need to be smaller than particle size while the filtration nanofiber need to be thicker than presently commercially available one. On the other hand, the tiny filtration pores or thick filtration channels has to cause higher airflow resistance, larger pressure drop, and the easy-to-block manner.

In order to resolve this contradiction fundamentally, here we demonstrate a conceptually new type of air filter for PM removal, which can work at high air flux with extremely low pressure drop. The conceptual illustration of this inertial filter is shown in Fig. 1(c). It can capture the PM particles suspended in air through a series of inertial separation processes. When a PM particle laden flow stream is caused to change direction suddenly, the PM particle with large mass will tend to follow an original trajectory due to the inertia effect. That is to say, traveling with hot exhausts, PM particles above a certain size possess so much inertial force that they cannot follow the air stream and finally impact with the adhesion layer which is used for capture. The concept of inertial impaction filter was firstly presented in 1955²¹. Over the years, various types of inertial impactors have been designed and developed, majority of which are low flow rate and designed for collection and monitoring of aerosol particles^{22–32}. Compared with traditionally commercial air filters, the filter channel of inertial impaction filter can be greatly enlarged, even dozens of times larger than average PM particle size, which can modify the easy-to-block intrinsic manner of traditional air filters. Besides, this inertial impaction filter can be made of various types of materials, which shows great potential for low-cost fabrication of large-area devices and the excellent thermal endurance and stability.

The inset of Fig. 1(c) demonstrates the cross-sectional illustration of an inertial impaction filter structure. The PM particle moves over the filtration channel, not through it as in filtration. Larger-size filtration channels will effectively avoid blocking during filtration process and also cut down the resistance of air mass, which will greatly improve the airflow rate and effectively reduce the frequency of blocking. We anticipate that these low-cost and easy-to-use inertial impaction would greatly benefit the public health in preventing PM air pollution.

Results and Discussions

According to the second law of Newton, the trajectory of a PM particle obeys the process that a particle mass multiplied by acceleration equals to the force exerted on it. In a fluid flow field, the PM particle will experience the Stokes drag force resulting from the relative velocity between particles and fluid flow field. Two-dimensional motion equations can be described by Equation 1³³,

$$\begin{aligned}\frac{Stk}{2} \frac{d^2x}{dt^2} &= u - \frac{dx}{dt} \\ \frac{Stk}{2} \frac{d^2y}{dt^2} &= v - \frac{dy}{dt},\end{aligned}\quad (1)$$

where (x, y) describes the instantaneous location of a particle at time t and (u, v) describes the instantaneous airflow velocity at point (x, y) , respectively. The Stokes number (Stk) is a dimensionless number characterizing the behavior of particles suspended in a fluid flow field. In order to precisely describe the trajectories of incident particles, we calculate the instantaneous velocity (u, v) of related flow field at every point based on the Navier-Stokes equation at first. Near the stagnation point, the convective term in the Navier-Stokes equation will be neglected due to the low Reynolds number ($Re < 1$) and then the fluid's Stokes equation may be solved by separation of variables. The instantaneous velocity of the flow field and related pressure at point (x, y) can be expressed as Equation 2. The detailed calculation is presented in Supplementary Material 1.

$$\begin{aligned}u &= 8xy \\ v &= -4y^2 \\ P &= -8uy,\end{aligned}\quad (2)$$

where (u, v) stands for the instantaneous velocity of the flow field and P stands for the pressure at point (x, y) , respectively. After a simple substitution of Equation 1, the trajectory of an incident particle inside inertial impaction filter can be mathematically expressed as Equation 3,

$$\begin{aligned}\frac{Stk}{2} \frac{d^2x}{dt^2} &= 8xy - \frac{dx}{dt} \\ \frac{Stk}{2} \frac{d^2y}{dt^2} &= -4y^2 - \frac{dy}{dt}.\end{aligned}\quad (3)$$

According to the fluid-dynamic theory, a particle with a low Stk will follow fluid streamlines while a particle with a large Stk will be dominated by its inertia and continues along its initial trajectory³⁴. Stk can be determined by Equation 4,

$$\begin{aligned}Stk &= \frac{Re}{9} \left(\frac{\rho_p}{\rho_f} + \frac{1}{2} \right) \times \left(\frac{d_p}{w} \right)^2 \\ Re &= \frac{\text{inertial forces}}{\text{viscous forces}} = \frac{\rho_f v w}{\mu} = \frac{u w}{\gamma},\end{aligned}\quad (4)$$

where ρ_p stands for the particle density, ρ_f stands for the density of air mass, d_p stands for the average dimension of a particle, u stands for the average inlet flow speed, w stands for the width of chamber inlet and γ stands for the kinematic viscosity of air mass, respectively. Re is defined as the ratio of inertial forces to viscous forces and consequently quantifies the relative importance of these two types of forces for given airflow conditions. For the common PM particles, the particle density (ρ_p) is estimated as 1000 kg/m³, the related air mass density (ρ_f) is approximated as 1.29 kg/m³, and the kinematic viscosity of the fluid (γ) for air is 1.8×10^{-5} Pa/s, respectively³⁵. As shown in Fig. 2, the trajectories of PM particles with different sizes are calculated according to Equation 3³³. By use of an inertia impaction filter with the inlet width of 20 μm , under the airflow velocity of 7.7 m/s, all the particles with aerodynamic diameter larger than 1.0 μm ($Stk \geq 1.79$) can be removed by inertial effect while no particles with diameter smaller than 0.95 μm ($Stk \leq 1.63$) impact with the collection plate. Through the precise control of the inlet width and related airflow velocity, the PM with sufficient inertia will slip across the sharply bending air streamlines and impact on adhesion layer while the finer particles will follow the bending air streamlines and move down stream of the impaction substrate. That is to say, traveling with hot exhausts, PM particles above a certain size possess so much mass and inertial force that they cannot follow the air stream and finally impact with the adhesion layer used for collection. By the similar calculation method, the relationship between incident velocity and designed width of chamber inlet can be concluded in Supplementary Material 2. Overall, the performance of an inertia filter can be predicted by numerical methods governing the fluid flow and particle

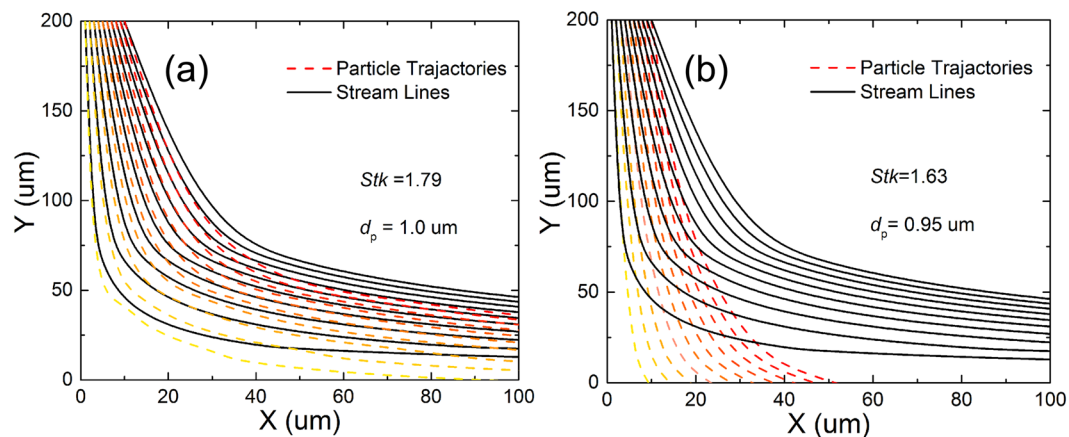


Figure 2. Particles' trajectories (red dashed lines) and airflow streamlines (black solid lines) calculated by use of the Stokes flow field when the size of particles is $1.0\ \mu\text{m}$ (a) and $0.95\ \mu\text{m}$ (b), respectively.

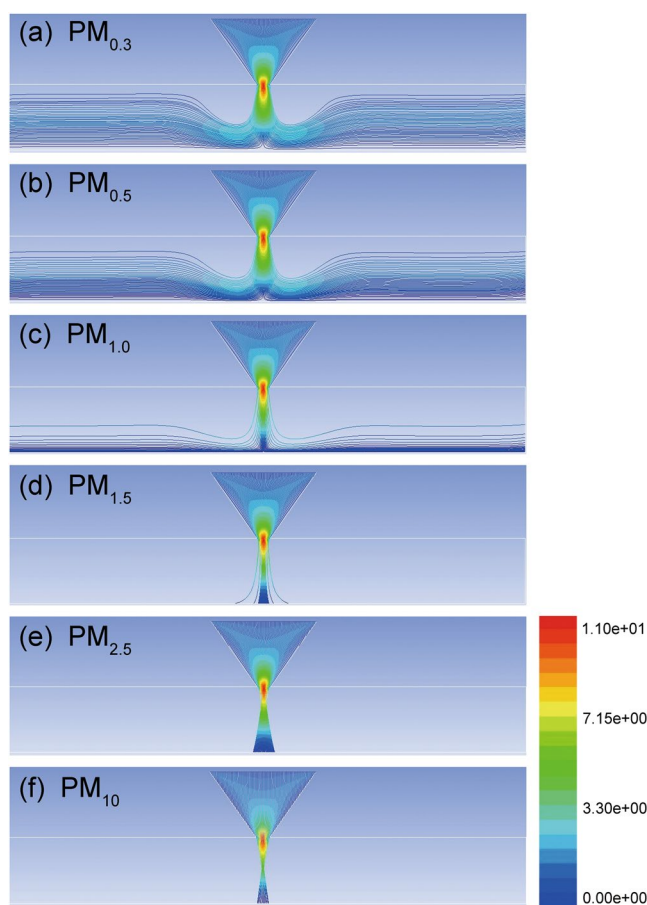


Figure 3. Trajectories of the PM particles with different sizes under the inlet velocity of $1.0\ \text{m/s}$.

motion. Several of analytical criterions about velocity have been developed for determining whether a particle is removed in Supplementary Material 3.

In additions, Navier-Stokes equation and Continuity equation are built and solved by use of the commercial code FLUENT. For PM particles with different sizes, the trajectories inside an inertial impaction filter can be simulated and traced for $1.0\ \text{m/s}$ inlet velocity as shown in Fig. 3 and for other inlet velocities as shown in Supplementary Material 4. Taking into account the gravity, Brownian motion, Saffman force, and pressure gradient, we calculate the related PM removal efficiency and pressure drop by use of the DPM model of FLUENT. With the increasing inlet velocities from $1.0\ \text{m/s}$ to $8.0\ \text{m/s}$, both the PM removal efficiencies (Supplementary Material 5) and the pressure drop (Supplementary Material 6) are gradually increased, respectively. Simulation

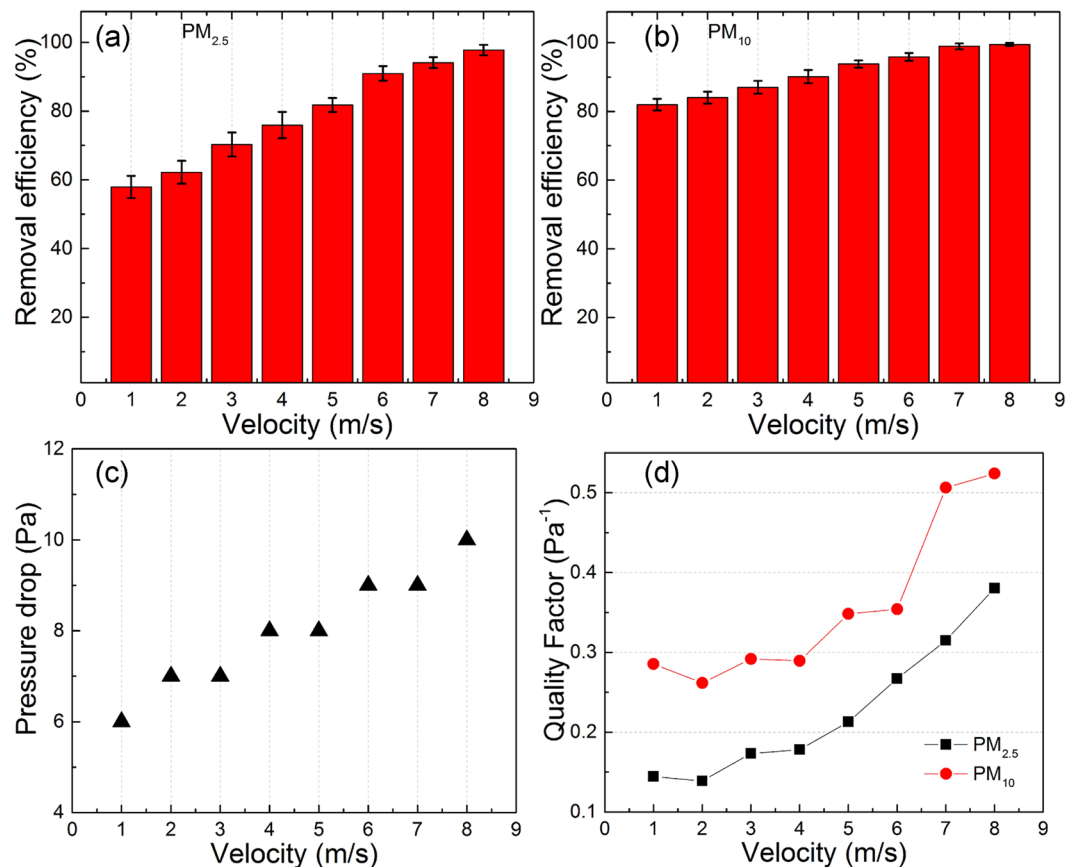


Figure 4. Removal efficiency of PM_{2.5} (a) and PM₁₀ (b), pressure drop (c), and quality factor (d) of the inertial impaction filters under different airflow velocities. Error bar represents the standard deviation of three replicate measurements.

results show the pressure drop is less than 100 Pa even with the inlet velocity of up to 8.0 m/s, which indicates great potential for rapid PM removal with the relatively low pressure drop.

The real inertial impaction filters are fabricated by the standard microfabrication processes in Biomolecular Nanotechnology Center at University of California at Berkeley. Detailed fabrication procedures are depicted in Methods section. Note that the whole fabrication processes meet the industry standard and are cost-effective and mass production compatible. In our case, the micro-size nozzle is fabricated on Si wafers. For the convenience of fast prototyping, the out-flow channel and collection part are fabricated on the polydimethylsiloxane (PDMS) substrate by using the soft lithography technology. Particularly worth mentioning is the material of these inertia impaction filters is very replaceable-flexible. Hence, the whole fabrication process indicates great potential for the low-cost fabrication of large-area devices and the excellent thermal endurance and stability.

In order to evaluate the PM filtration performance, we design and fabricate a home-made measurement protocol. Detailed measuring process are depicted in Methods section. The PM source used here is generated by the burning of cigarettes and collected into a stainless steel reactor. The FT-IR analysis of the cigarette ashes confirms that the ingredients of smoke from burning cigarettes can be analogous to those of PM_{2.5} pollution (Supplementary Material 7). We consider that the cigarette ash illustrates a cognate spectrum to that of PM pollutants suspended in air. So in this work we choose the smoke from burning cigarettes as representative source PM. Note that the cigarette smoke PM particles have a wide size distribution from smallest size around 0.1 μm to largest size bigger than 10 μm , while the average size is 1.0 μm or less. With the increasing airflow velocity, both the removal efficiencies of PM_{2.5} and PM₁₀ exhibit a slow increase as shown in Fig. 4(a) and (b) while the corresponding pressure drop curves shift upwards continuously as shown in Fig. 4(c). Under the airflow velocity of 8.0 m/s, Fig. 4(d) shows the inertial impaction filters show high PM removal efficiencies up to $97.77 \pm 1.53\%$ and $99.47 \pm 0.45\%$ for PM_{2.5} and PM₁₀, respectively. Compared with the traditional air filters reported previously, the pressure drop is as low as 5–10 Pa. The extremely low pressure drop of our inertial impaction filter gives rise to greatly improved filtration performance, which can be evaluated regularly by a trade-off parameter named quality factor (QF)^{36,37}. In comparison with the available literatures as shown in Table 1, our inertial impaction filter exhibits highly improved filtration performance achieved by largest QF values and extremely low pressure drop. We anticipate that there are no fundamental obstacles to extending these new techniques to PM filtrations at higher airflow velocity and this inertial impaction filter will be a start point for future low-cost, high-efficiency, and durable air filter with good thermos-stability, extremely low airflow resistance, and long operation life.

Materials	QF^a value (Pa^{-1})	Δp^b for different flow rates(Pa)	E^c (%)	Test particles	Additional advantages	Ref.
PAN nanofiber	0.024	133 Pa for 3 m/s	96.12	$\text{PM}_{2.5}$	~85% transparency	10
PI nanofiber	0.1072	73 Pa for 0.2 m/s	99.97	$\text{PM}_{2.5}$	~370°C thermal stability	17
PAN nanofiber	0.1014	80 Pa for 0.2 m/s	99.97	$\text{PM}_{2.5}$	~230°C thermal stability	17
Nylon-6 nanofiber	0.062	42 Pa for 0.2 m/s	92.73	$\text{PM}_{2.5}$	~10 times faster production speed	38
PAN nanofiber	0.052	124 Pa for 0.6~0.8 m/s	99.86	$\text{PM}_{2.5}$	Large-scale direct coating	39
R-TENG ^d enhanced PI nanofiber	—	17 Pa for 1 m/s 180 Pa for 5 m/s	97	PM	—	40
Nanofibrous MOF ^e	—	20 Pa for 50 mL/min	88.33 89.67	$\text{PM}_{2.5}$ PM_{10}	—	41
PVDF ^f nanofibers with NIPS ^g	0.042	95 Pa for 0.0166 m/s	98.33	$\text{PM}_{2.5}$	Releasing negative ions	42
PVDF/PAN	0.0954	45 Pa for 14 L/min	98.34	$\text{PM}_{2.5}$	Rapidly transferring moisture	43
Commercial-1	0.00062	299 Pa	16.93	$\text{PM}_{2.5}$	—	10
Commercial-2	0.0068	809 Pa	99.58	$\text{PM}_{2.5}$	—	10
This work	0.380 0.524	10 Pa for 8.0 m/s	97.77 99.47	$\text{PM}_{2.5}$ PM_{10}	Extremely low airflow resistance and pressure drop	

Table 1. A summary of performances of different materials and designs for PM filtration in recent literatures in comparison to what is achieved in this work. ^a QF stands for the quality factor, $QF = -\ln(1 - E\%)/\Delta p$. ^b Δp stands for the pressure drop. ^c E stands for the PM removal efficiency. ^dR-TENG stands for the rotating triboelectric nano generator. ^eMOF stands for the metal organic framework. ^fPVDF stands for the polyvinylidene fluoride. ^gNIPs stands for the negative ions powders.

In summary, the design and fabrication process of a conceptually new type of air filter is demonstrated in detail. Under the airflow velocity of 8.0 m/s, the real inertial impaction filters show high PM removal efficiencies of up to $97.77 \pm 1.53\%$ and $99.47 \pm 0.45\%$ for $\text{PM}_{2.5}$ and PM_{10} , respectively. Compared with traditional filters, inertia impaction filters also exhibit extremely low pressure drop of 5–10 Pa and greatly improved quality factor values of up to 0.380 Pa^{-1} for $\text{PM}_{2.5}$ and 0.524 Pa^{-1} for PM_{10} , respectively. Meanwhile, the analysis and simulation of the filter efficiency and pressure drop paves the way for future research into designs of inertia impaction filters. In particular, this inertial structure can be made of various types of materials with excellent thermal endurance and stability, which shows great potential for low-cost fabrication of large-area devices. We consider that these inertia impaction filters can work both independently and work together with traditional filters as a pretreatment equipment to achieve a healthier public living environment.

Methods

The real inertial impaction filters are fabricated by the standard microfabrication techniques, as depicted in Supplementary Material 8. For the nozzle part of inertial impaction filter, fabrication process begins with prime grade, double-sided polished, ultrathin Si wafers with $\langle 100 \rangle$ orientation. Starting from cleaning by Piranha, wafers are air dried and deposited stoichiometric silicon nitride (SiN_x) by LPCVD method on both sides. Next, photolithography process is carried out to pattern the shape of nozzle. When the pattern is generated, CF_4/O_2 plasma etching is conducted to generate SiN_x mask by use of patterned photoresist as a protect layer. Then, the photoresist is stripped away by soaking in 90 °C heated PRS-3000 bath. Wafers are cleaned and dried by N_2 gun after stripping. Subsequently, the nozzle is generated by use of KOH solution etching. KOH bath has a great selectivity toward SiN_x and Si so the SiN_x mask kept well during wet etching. After wet etching, wafers will soak into $\text{HCl}/\text{H}_2\text{O}_2$ solution to remove metal ions for 2 hours and then be washed by deionized water and dried by N_2 gun again. Next, the residual SiN_x is removed by CF_4/O_2 plasma etching. Served to exhaust the gas stream, the bottom part is made by use of soft lithography technology. Finally, the Si-based nozzle and PDMS-based bottom part are assembled together.

As depicted in Supplementary Material 9, the inertial impaction filter is placed in the air inlet and sealed with double-sided adhesive tape to make sure the source PM passing into the transparent chamber completely. PM particle number concentrations are detected by use of a professional PM counter (PureAir, China) placed inside of transparent chamber, and the pressure drop is measured by use of an electronic pressure transmitters. The removal efficiency is defined by comparing the particle number concentrations before and after filtration, and the airflow velocity is tested by an anemometer.

References

- Zhang, Q. *et al.* Transboundary health impacts of transported global air pollution and international trade. *Nature* **543**, 705–709 (2017).
- Nel, A. Air Pollution–Related illness: effects of particles. *Science* **308**, 804–806 (2005).
- Mathowald, N. Aerosol indirect effect on biogeochemical cycles and climate. *Science* **334**, 794–796 (2011).
- He, M. *et al.* Urban $\text{PM}_{2.5}$ exacerbates allergic inflammation in the murine lung via a TLR2/TLR4/MyD88-signaling pathway. *Sci. Rep.* **7**, 11027 (2017).
- Horton, D., Skinner, C., Singh, D. & Duffenbaugh, N. Occurrence and persistence of future atmospheric stagnation events. *Nat. Clim. Change* **4**, 698–703 (2014).
- Maji, K. J., Dikshit, A. K., Arora, M. & Deshpande, A. Estimating premature mortality attributable to $\text{PM}_{2.5}$ exposure and benefit of air pollution control policies in China for 2020. *Sci. Total Environ.* **26**, 244 (2018).
- Rao, C. *et al.* Capturing $\text{PM}_{2.5}$ emissions from 3D printing via nanofiber-based air filter. *Sci. Rep.* **7**, 10366 (2017).

8. Qin, X. & Wang, S. Filtration properties of electrospinning nanofibers. *J. Appl. Polym. Sci.* **102**, 1285–1290 (2006).
9. Qin, X. & Wang, S. Electrospun nanofibers from crosslinked poly(vinyl alcohol) and its filtration efficiency. *J. Appl. Polym. Sci.* **109**, 951–958 (2008).
10. Liu, C. *et al.* Transparent air filter for high-efficiency PM_{2.5} capture. *Nat. Commun.* **6**, 6205 (2015).
11. Nataraj, S., Yang, K. & Aminabhavi, T. Polyacrylonitrile-based nanofibers a state-of-the-art review. *Prog. Polym. Sci.* **37**, 487–513 (2012).
12. Su, S. *et al.* Ultra-thin electro-spun PAN nanofiber membrane for high-efficient inhalable PM_{2.5} particles filtration. *J. Nano. Res.* **46**, 73–81 (2017).
13. Strain, I. *et al.* Electrospinning of recycled PET to generate tough mesomorphic fiber membranes for smoke filtration. *J. Mater. Chem. A* **3**, 1632–1640 (2015).
14. Sambaer, W., Zatloukal, M. & Kimmer, D. 3D modeling of filtration process via polyurethane nanofiber based nonwoven filters prepared by electrospinning process. *Chem. Eng. Sci.* **66**, 613–623 (2011).
15. Wang, Z., Zhao, C. & Pan, Z. Porous bead-on-string poly (lactic acid) fibrous membranes for air filtration. *J. Colloid Interface Sci.* **441**, 121–129 (2015).
16. Wang, N., Wang, X., Ding, B., Yu, J. & Sun, G. Tunable fabrication of three-dimensional polyamide-66 nano-fiber/nets for high efficiency fine particulate filtration. *J. Mater. Chem.* **22**(4), 1445–1452 (2011).
17. Zhang, R. *et al.* Nanofiber air filters with high-temperature stability for efficient PM_{2.5} removal from the pollution sources. *Nano Lett.* **16**(6), 3642–3649 (2016).
18. Wang, N. *et al.* Multilevel structured polyacrylonitrile/silica nanofibrous membranes for high-performance air filtration. *Sep. Purif. Technol.* **126**, 44–51 (2014).
19. Wan, H. *et al.* Hierarchically structured polysulfone/titania fibrous membranes with enhanced air filtration performance. *J. Colloid Interface Sci.* **417**, 18–26 (2014).
20. Wang, Z., Pan, Z., Wang, J. & Zhao, R. A. Novel hierarchical structured poly (lactic acid)/titania fibrous membrane with excellent antibacterial activity and air filtration performance. *J. Nanomater.* **2016**, 39 (2016).
21. Wong, J. B., Ranz, W. E. & Johnstone, H. F. Inertial impaction of aerosol particles on cylinders. *J. Appl. Phys.* **26**, 244 (1955).
22. McFarland, A. R., Ortiz, C. A. & Bertsch, R. W. J. Particle collection characteristics of a single stage dichotomous sampler. *Environ. Sci. Technol.* **12**, 679–682 (1978).
23. Sioutas, C., Ferguson, S. T., Wolfson, J. M., Ozkaynak, H. & Koutrakis, P. Inertial collection of fine particles using a high-volume rectangular geometry conventional impactor. *J. Aerosol Sci.* **28**, 1015–1028 (1997).
24. Demokritou, P., Kavouras, I. G., Ferguson, S. T. & Koutrakis, P. Development and laboratory performance evaluation of personal multipollutant sampler for simultaneous measurement of particle and gaseous pollutants. *Aerosol Sci. Technol.* **35**, 741–752 (2001).
25. Misra, C., Singh, M., Shen, S., Sioutas, C. & Hall, P. M. Development and valuation of a personal cascade impactor sampler. *J. Aerosol Sci.* **33**, 1027–1047 (2002).
26. Lee, S. J., Demokritou, P., Koutrakis, P. & Delgado-Saborit, J. M. Development and evaluation of personal respirable particulate sampler. *Atmos. Environ.* **40**, 212–224 (2006).
27. Singh, S., Sapra, B. K., Khan, A., Kothalkar, P. K. & Mayya, Y. S. Development of a variable configuration cascade impactor for aerosol size distribution measurement. *Atmos. Environ.* **44**, 795–802 (2010).
28. Ihanlainen, M. *et al.* Experimental study on bounce of submicron agglomerates upon inertial impaction. *Powder Technol.* **268**, 203–209 (2014).
29. Zaripov, S. K., Soloveva, O. V. & Solovev, S. A. Inertial deposition of aerosol particles in a periodic row of porous cylinders. *Aerosol Sci. Technol.* **49**, 400–408 (2015).
30. Cheon, T. W., Lee, J. Y., Bae, J. Y. & Yook, S. J. Enhancement of collection efficiency of an inertial impactor using an additional punched impaction plate. *Aerosol Air Qual. Res.* **17**(10), 2349–2357 (2017).
31. Huang, H. K., Zheng, C. H. & Zhao, H. B. Numerical investigation on on-steady-state filtration of elliptical fibers for submicron particles in the “Greenfield gap” range. *J. Aerosol Sci.* **114**, 263–275 (2017).
32. Chen, X. L., Feng, Y., Zhong, W. Q., Sun, B. B. & Tao, F. Numerical investigation of particle deposition in a triple bifurcation airway due to gravitational sedimentation and inertial impaction. *Powder Technol.* **323**, 284–293 (2018).
33. Niu, F., Du, X., Qi, H., Yi, M. & Yang, X. Modeling analyses of radioactive aerosol flow and collection in mesoscopic impactor filters. *Prog. Nucl. Energ.* **88**, 147–155 (2016).
34. Taylor, C. & Hood, P. A numerical solution of the Navier-Stokes equations using the finite element technique. *Comput. Fluids* **1**(1), 73 (1973).
35. Lietz, A., Johnsen, E. & Kushner, M. Plasma-induced flow instabilities in atmospheric pressure plasma jets. *Appl. Phys. Lett.* **111**, 114101 (2017).
36. Chen, C. Y. Filtration of aerosols by fibrous media. *Chem. Rev.* **55**, 595–623 (1955).
37. Li, P., Wang, C., Zhang, Y. & Wei, F. Air filtration in the free molecular flow regime: a review of high-efficiency particulate air filters based on carbon nanotubes. *Small* **10**(22), 4543–4561 (2014).
38. Xu, J. *et al.* Roll-to-roll transfer of electrospun nanofiber film for high-efficiency transparent air filter. *Nano Lett.* **16**, 1270–1275 (2016).
39. Khalid, B. *et al.* Direct blow-spinning of nanofibers on a window screen for highly efficient PM_{2.5} removal. *Nano Lett.* **17**(2), 1140–1148 (2017).
40. Gu, G. *et al.* Triboelectric nanogenerator enhanced nanofiber air filters for efficient particulate matter removal. *ACS Nano* **11**(6), 6211–6217 (2017).
41. Zhang, Y. *et al.* Preparation of nanofibrous metal-organic framework filters for efficient air pollution control. *J. Am. Chem. Soc.* **138**, 5785–5788 (2016).
42. Zhao, X. *et al.* Low-resistance dual-purpose air filter releasing negative ions and effectively capturing PM_{2.5}. *ACS Appl. Mater. Interfaces* **9**, 12054–12063 (2017).
43. Zhao, X. *et al.* Cleanable air filter transferring moisture and effectively capturing PM_{2.5}. *Small* **13**(11), 1603306 (2017).

Acknowledgements

This work was supported by National Natural Science Foundation of China (NSFC) (61704094, 11635005, 61735008, 11774155, and 61474068), Priority Academic Program Development of Jiangsu Higher Education Institutions (PAPD), and K. C. Wong Magna Fund in Ningbo University. We thank Dr. Paul Lum from Biomolecular Nano Center at University of California at Berkeley for the fabrications of inertia impaction filters.

Author Contributions

P.W., F.N. and J.X. designed and supervised the entire study. X.Z. and Y.W. fabricated a series of inertial impaction filters and performed the related PM measurements. W.Z. and F.N. simulated the whole filter processes and designed the prototype devices. X.Z. and M.Y. setup the PM filtration efficiency measurement. X.Z. and W.Z. wrote the manuscript. J.X. and F.L. revised the manuscript. All authors did a favor for the final manuscript.

Additional Information

Supplementary information accompanies this paper at <https://doi.org/10.1038/s41598-018-23257-x>.

Competing Interests: The authors declare no competing interests.

Publisher's note: Springer Nature remains neutral with regard to jurisdictional claims in published maps and institutional affiliations.



Open Access This article is licensed under a Creative Commons Attribution 4.0 International License, which permits use, sharing, adaptation, distribution and reproduction in any medium or format, as long as you give appropriate credit to the original author(s) and the source, provide a link to the Creative Commons license, and indicate if changes were made. The images or other third party material in this article are included in the article's Creative Commons license, unless indicated otherwise in a credit line to the material. If material is not included in the article's Creative Commons license and your intended use is not permitted by statutory regulation or exceeds the permitted use, you will need to obtain permission directly from the copyright holder. To view a copy of this license, visit <http://creativecommons.org/licenses/by/4.0/>.

© The Author(s) 2018